Measurement of production properties of positively charged kaons in proton-carbon interactions at 31 GeV/*c*

NA61/SHINE Collaboration

ABGRALL, Nicolas (Collab.), *et al*.

Abstract

Spectra of positively charged kaons in p+C interactions at 31 GeV/c were measured with the NA61/SHINE spectrometer at the CERN SPS. The analysis is based on the full set of data collected in 2007 with a graphite target with a thickness of 4% of a nuclear interaction length. Interaction cross sections and charged pion spectra were already measured using the same set of data. These new measurements in combination with the published ones are required to improve predictions of the neutrino flux for the T2K long-baseline neutrino oscillation experiment in Japan. In particular, the knowledge of kaon production is crucial for precisely predicting the intrinsic electron neutrino component and the high-energy tail of the T2K beam. The results are presented as a function of laboratory momentum in two intervals of the laboratory polar angle covering the range from 20 to 240 mrad. The kaon spectra are compared with predictions of several hadron production models. Using the published pion results and the new kaon data, the K+/π+ ratios are computed.

UNIVERSITÉ
DE GENÈVE

Measurement of production properties of positively charged kaons in proton-carbon interactions at 31 GeV/c

N. Abgrall,[1] A. Aduszkiewicz,[2] T. Anticic,[3] N. Antoniou,[4] J. Argyriades,[1] B. Baatar,[5] A. Blondel,[1] J. Blumer,[6] M. Bogusz,[7] L. Boldizsar,[8] A. Bravar,[1] W. Brooks,[9] J. Brzychczyk,[10] A. Bubak,[11] S. A. Bunyatov,[5] O. Busygina,[12] T. Cetner,[7] K.-U. Choi,[13] P. Christakoglou,[4] T. Czopowicz,[7] N. Davis,[4] F. Diakonos,[4] S. Di Luise,[15] W. Dominik,[2] J. Dumarchez,[16] R. Engel,[6] A. Ereditato,[17] L. S. Esposito,[15] G. A. Feofilov,[18] Z. Fodor,[8] A. Ferrero,[1] A. Fulop,[8] X. Garrido,[6] M. Gaździcki,[19,20] M. Golubeva,[12] K. Grebieszkow,[7] A. Grzeszczuk,[11] F. Guber,[12] A. Haesler,[1] H. Hakobyan,[9] T. Hasegawa,[21] R. Idczak,[22] Y. Ivanov,[9] A. Ivashkin,[12] K. Kadija,[3] A. Kapoyannis,[4] N. Katryńska,[22] D. Kiełczewska,[2] D. Kikola,[7] J.-H. Kim,[13] M. Kirejczyk,[2] J. Kisiel,[11] T. Kobayashi,[21] O. Kochebina,[18] V. I. Kolesnikov,[5] D. Kolev,[23] V. P. Kondratiev,[18] A. Korzenev,[1] S. Kowalski,[11] A. Krasnoperov,[5] S. Kuleshov,[9] A. Kurepin,[12] R. Lacey,[14] J. Lagoda,[24] A. Laszlo,[8] V. V. Lyubushkin,[5] M. Maćkowiak-Pawłowska,[7] Z. Majka,[10] A. I. Malakhov,[5] A. Marchionni,[15] A. Marcinek,[10] I. Maris,[6] V. Marin,[12] T. Matulewicz,[2] V. Matveev,[12,5] G. L. Melkumov,[5] A. Meregaglia,[15] M. Messina,[17] St. Mrówczyński,[19] S. Murphy,[1] T. Nakadaira,[21] K. Nishikawa,[21] T. Palczewski,[24] G. Palla,[8] A. D. Panagiotou,[4] T. Paul,[6] W. Peryt,[7] O. Petukhov,[12] R. Płaneta,[10] J. Pluta,[7] B. A. Popov,[5,16] M. Posiadała,[2] S. Puławski,[11] W. Rauch,[25] M. Ravonel,[1] R. Renfordt,[20] A. Robert,[16] D. Röhrich,[26] E. Rondio,[24] B. Rossi,[17] M. Roth,[6] A. Rubbia,[15] M. Rybczyński,[19] A. Sadovsky,[12] K. Sakashita,[21] T. Sekiguchi,[21] P. Seyboth,[19] M. Shibata,[21] E. Skrzypczak,[2] M. Słodkowski,[7] P. Staszel,[10] G. Stefanek,[19] J. Stepaniak,[24] C. Strabel,[15] H. Ströbele,[20] T. Susa,[3] P. Szaflik,[11] M. Szuba,[6] M. Tada,[21] A. Taranenko,[14] V. Tereshchenko,[5] R. Tsenov,[23] L. Turko,[22] R. Ulrich,[6] M. Unger,[6] M. Vassiliou,[4] D. Veberič,[6] V. V. Vechernin,[18] G. Vesztergombi,[8] A. Wilczek,[11] Z. Włodarczyk,[19] A. Wojtaszek-Szwarć,[19] J.-G. Yi,[13] I.-K. Yoo,[13] L. Zambelli,[16] and W. Zipper[11]

(NA61/SHINE Collaboration)

[1]*University of Geneva, Geneva, Switzerland*
[2]*Faculty of Physics, University of Warsaw, Warsaw, Poland*
[3]*Rudjer Boskovic Institute, Zagreb, Croatia*
[4]*University of Athens, Athens, Greece*
[5]*Joint Institute for Nuclear Research, Dubna, Russia*
[6]*Karlsruhe Institute of Technology, Karlsruhe, Germany*
[7]*Warsaw University of Technology, Warsaw, Poland*
[8]*KFKI Research Institute for Particle and Nuclear Physics, Budapest, Hungary*
[9]*Universidad Tecnica Federico Santa Maria, Valparaiso, Chile*
[10]*Jagiellonian University, Cracow, Poland*
[11]*University of Silesia, Katowice, Poland*
[12]*Institute for Nuclear Research, Moscow, Russia*
[13]*Pusan National University, Pusan, Republic of Korea*
[14]*State University of New York, Stony Brook, New York, USA*
[15]*ETH, Zurich, Switzerland*
[16]*LPNHE, University of Paris VI and VII, Paris, France*
[17]*University of Bern, Bern, Switzerland*
[18]*St. Petersburg State University, St. Petersburg, Russia*
[19]*Jan Kochanowski University in Kielce, Poland*
[20]*University of Frankfurt, Frankfurt, Germany*
[21]*High Energy Accelerator Research Organization (KEK), Tsukuba, Ibaraki 305-0801, Japan*
[22]*University of Wrocław, Wrocław, Poland*
[23]*Faculty of Physics, University of Warsaw, Warsaw, Poland*
[24]*National Centre for Nuclear Research, Warsaw, Poland*
[25]*Fachhochschule Frankfurt, Frankfurt, Germany*
[26]*University of Bergen, Bergen, Norway*

Spectra of positively charged kaons in $p + $C interactions at 31 GeV/c were measured with the NA61/SHINE spectrometer at the CERN SPS. The analysis is based on the full set of data collected in 2007 with a graphite target with a thickness of 4% of a nuclear interaction length. Interaction cross sections and charged pion spectra were already measured using the same set of data. These new measurements in combination with the published ones are required to improve predictions of the neutrino flux for the T2K long-baseline neutrino oscillation experiment in Japan. In particular, the knowledge of kaon production is crucial for precisely predicting the intrinsic electron neutrino component and the high-energy tail of the T2K beam. The results are presented as

a function of laboratory momentum in two intervals of the laboratory polar angle covering the range from 20 to 240 mrad. The kaon spectra are compared with predictions of several hadron production models. Using the published pion results and the new kaon data, the K^+/π^+ ratios are computed.

I. INTRODUCTION

The Super Proton Synchrotron (SPS) Heavy Ion and Neutrino Experiment (NA61/SHINE) at CERN pursues a rich physics program [1–4]. Hadron production measurements in $p + C$ and $\pi + C$ interactions will improve calculations of neutrino fluxes in the T2K experiment [5] and simulations of cosmic-ray air showers in the Pierre Auger and KASCADE experiments [6,7]. The heavy ion program investigates $p + p$, $p + Pb$, and nucleus+nucleus collisions at SPS energies, to study the onset of deconfinement and search for the critical point of strongly interacting matter. Charged pion spectra in $p + C$ interactions at 31 GeV/c were already published [8] and used for neutrino flux prediction in T2K [9]. The measurement is performed on the data collected during the first running period in 2007. This paper presents measurements of positively charged kaon spectra in $p + C$ interactions at 31 GeV/c, based on the same 2007 set of data.

A detailed description of the experimental apparatus and analysis techniques can be found in Ref. [8].

T2K—the long baseline neutrino experiment from J-PARC in Tokai to Kamioka (Japan)—aims to precisely measure the $\nu_\mu \to \nu_e$ appearance and ν_μ disappearance [5,9]. The neutrino beam is generated by the J-PARC high-intensity 30-GeV (kinetic energy) proton beam interacting in a 90-cm-long graphite target to produce π and K mesons, which decay by emitting neutrinos. The resulting neutrino beam is aimed toward a near-detector complex, 280 m from the target, and to the Super-Kamiokande (SK) far detector located 295 km away at 2.5 degrees off axis from the hadron beam. Neutrino oscillations are probed by comparing the neutrino event rates measured in SK to the predictions of a Monte Carlo simulation based on flux calculations and near-detector measurements. Until the NA61/SHINE data were available, these flux calculations were based on hadron production

models tuned to sparse available data, resulting in systematic uncertainties which are large and difficult to evaluate. Direct measurement of particle production rates in $p + C$ interactions allows more precise and reliable estimates. Presently, the T2K neutrino beam line is set up to focus positively charged hadrons, to produce a ν_μ beam. While charged pions generate most of the low-energy neutrinos, positively charged kaons generate the high-energy tail of the T2K beam and contribute substantially to the intrinsic ν_e component in the T2K beam.

Positively charged kaons whose daughter neutrinos pass through the SK detector constitute the kinematic region of interest, shown in Fig. 1, in the kinematic variables p and θ—the momentum and polar angle of particles in the laboratory frame. The low statistics available in the 2007 pilot data set imposes a p, θ binning which covers only the most populated region of phase space relevant for T2K. Moreover, the statistics of the 2007 data does not allow for measurements of negatively charged kaons. An order of magnitude larger data set was recorded in 2009, and, when analyzed, will lead to essentially full coverage. The NA61/SHINE data on kaon production will allow us also to test and improve existing hadron production models in an energy region which is not well constrained by measurements at present. Several K^+ production measurements in this energy range were performed previously [10–16].

II. THE EXPERIMENTAL SETUP

The NA61/SHINE apparatus (the details of which are described in Ref. [8], Sec. II) is a wide acceptance spectrometer made of four large-volume time projection chambers (TPCs): two vertex TPCs (VTPC-1 and VTPC-2) placed in the magnetic field produced by two superconducting dipole magnets and two main TPCs (MTPC) located downstream symmetrically with respect to the beam line (Fig. 2). In the forward region, the setup is complemented by a time-of-flight (ToF-F) detector array horizontally segmented into 64 scintillator bars read out at both ends by photomultipliers. The time resolution of each scintillator is about 115 ps [17]. For the study presented here the magnetic field was set to a bending power of 1.14 Tm. This leads to a momentum resolution $\sigma(p)/p^2$ in the track reconstruction of about 5×10^{-3} (GeV/c)$^{-1}$. The target used is an isotropic graphite sample with a thickness along the beam axis of 2 cm, equivalent to about 4% of a nuclear interaction length, λ_I. During the data taking the target was placed 80 cm upstream of VTPC-1.

III. ANALYSIS TECHNIQUE

This section presents details on data selection and binning, the kaon identification method as well as corrections and systematic errors.
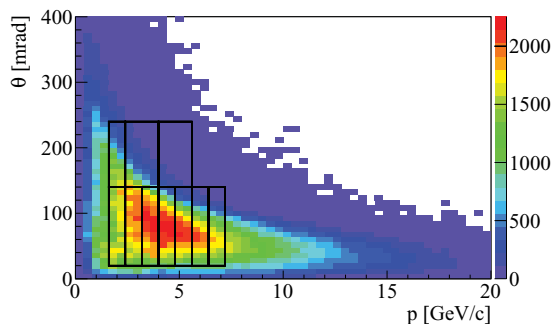

FIG. 1. (Color online) The prediction from the T2K beam simulation; the $\{p, \theta\}$ distribution for positively charged kaons weighted by the probability that their decay produces a neutrino passing through the SK detector. The binning used in the present analysis is superimposed; the kinematic range considered is $1.6 < p < 7.2$ GeV/c and $20 < \theta < 240$ mrad.
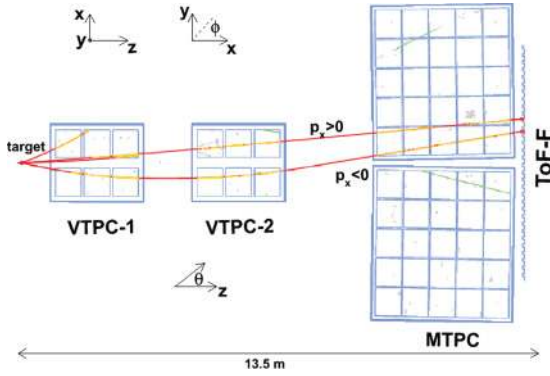
FIG. 2. (Color online) Schematic drawing of the experimental apparatus (Sec. II) and a reconstructed $p + C$ interaction event. Yellow (green) points indicate TPC clusters (not) associated with reconstructed primary tracks. Stars correspond to hits reconstructed in the ToF-F. Red lines are the fitted particle trajectories.

A. Data binning

The adopted binning scheme is mainly driven by the available statistics and is presented in Fig. 1. Details can be found in Table I. The highest θ limit is determined by the requirement for the track to be in the geometrical acceptance of the ToF-F detector.

Only two angular intervals are defined. The lowest θ value is set to 20 mrad in order to exclude tracks passing close to the edges of the TPCs where the reconstruction efficiency is lower and the calculation of the correction for the acceptance is less reliable. The first angular interval extends up to 140 mrad so as to cover most of the T2K relevant θ range and, combined with a 0.8 GeV/c momentum bin width, to have a few thousand selected tracks per interval (Table I). Measurements were performed up to 7.2 GeV/c. This choice comes from the fact that in the relativistic rise region (above 4–5 GeV/c) particle identification requires extracting the rapidly decreasing kaon signal from the predominant proton one. With the available

statistics of 2007 data the applied procedure turned out to be robust only up to about 7 GeV/c.

B. Event and track selection

This analysis is based on 452×10^3 reconstructed events collected during the 2007 data taking. Only events for which a beam track is properly reconstructed are selected. The beam trajectory is measured with a set of beam position detectors (BPDs) placed upstream of the target (see [8], Secs. III and V). The following criteria were applied to select well-measured positively charged tracks in the TPCs and ensure high reconstruction efficiency as well as to reduce the contamination of tracks from secondary interactions:

(i) The track momentum fit at the interaction vertex should have converged.
(ii) A minimum of 12 reconstructed points in the two TPCs used for momentum measurement, VTPC-1 and VTPC-2, is required.
(iii) The distance of closest approach of the fitted track to the interaction point (impact parameter) is required to be smaller than 4 cm in both transverse directions.
(iv) The track must leave the primary vertex at an azimuthal angle ϕ within $\pm 20°$ around the horizontal plane, for the first θ interval, and $\pm 10°$ for the second; this excludes most of the tracks traversing the detector in the regions where the reconstruction capability is limited by the magnet aperture or by the presence of uninstrumented regions in the VTPCs,
(v) The track must have an associated ToF-F hit.

The position of a ToF-F hit is determined only in the x direction and with a precision given by the width of the scintillator slat producing the signal ($\sim$10 cm) (Fig. 2). A ToF-F hit is then associated with a track if the trajectory can be extrapolated to the pertaining slat.

TABLE I. The NA61/SHINE results for the differential K^+ production cross section in the laboratory system, $d\sigma/dp$, and the K^+ to π^+ ratio of production cross sections, $\sigma^{K^+}/\sigma^{\pi^+}$, for $p + C$ interactions at 31 GeV/c. Each row refers to a different ($p_{low} \leqslant p < p_{up}$, $\theta_{low} \leqslant \theta < \theta_{up}$) bin, where p and θ are the kaon momentum and polar angle in the laboratory frame. N is the total number of selected tracks and N_K is the fitted raw number of kaons. The central value and the statistical (Δ_{stat}) and systematic (Δ_{sys}) errors of the cross section are given. The overall uncertainty (2.5%) due to the normalization procedure is not included. For the K^+/π^+ ratio, errors are calculated by taking into account only statistical uncertainties.

| θ_{low}	θ_{high}	p_{low}	p_{high}	N	N_K	$d\sigma^{K^+}/dp$	Δ_{stat}	Δ_{sys}	$\sigma^{K^+}/\sigma^{\pi^+}$	Δ_{stat}
(mrad)		(GeV/c)				[mb/(GeV/c)]				
20	140	1.6	2.4	2395	56	1.94	0.26	0.07	0.062	0.008
		2.4	3.2	2934	106	2.25	0.21	0.08	0.082	0.008
		3.2	4	2662	134	2.39	0.22	0.08	0.10	0.01
		4	4.8	2263	127	2.10	0.20	0.08	0.11	0.01
		4.8	5.6	1964	126	1.94	0.18	0.07	0.13	0.01
		5.6	6.4	1699	97	1.49	0.17	0.05	0.12	0.01
		6.4	7.2	1424	81	1.17	0.17	0.08	0.13	0.02
140	240	1.6	2.4	1399	49	2.89	0.41	0.11	0.11	0.02
		2.4	4	1340	64	1.32	0.17	0.06	0.12	0.02
		4	5.6	529	32	0.55	0.12	0.06	0.20	0.04
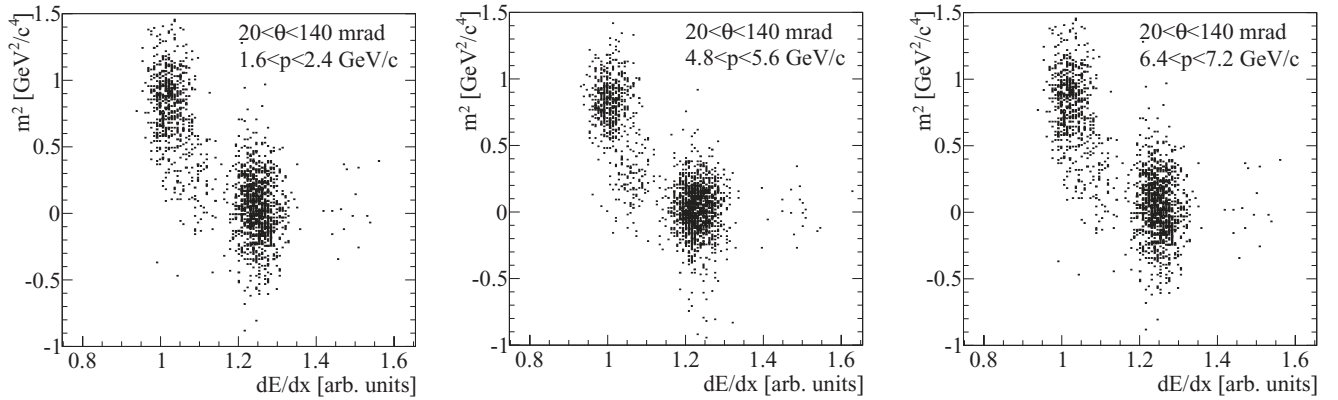
FIG. 3. Scatter plots of dE/dx vs m^2 measured for the selected tracks in three $\{p, \theta\}$ bins.

The relatively short proper decay length of kaons ($c\tau \sim$ 3.7 m) compared to the longitudinal extension of the detector ($\sim$13 m) implies that almost 60% of these particles produced in the target at the lowest laboratory momentum considered, 1.6 GeV/c, decay before reaching the ToF-F detector array.

Thanks to the high Q values of the kaon decay channels, kink topologies are correctly reconstructed as a primary and a secondary track (i.e., not fitted to the primary vertex) with an efficiency higher than 98%. Nevertheless, a ToF-F hit would still be associated with a kaon decaying in flight if the secondary particle produces a hit along the same scintillator bar in which a hit from the primary is expected. As a consequence the time of flight measurement could be significantly biased. Such special topologies can be effectively rejected by considering only tracks reconstructed until the downstream edge of the MTPCs. (see Sec. III D). This can be achieved by the following cut:

(i) The z position of the last reconstructed point, z_{last}, must differ by less than 50 cm from the position of the last potential point (see also Fig. 2).

The sample can be divided into tracks emitted in the same direction in which they are bent by the magnetic field (i.e., $p_x > 0$ for positive charges) and tracks emitted in the opposite direction (see Fig. 2). These two independent subsamples were treated separately. In fact, for the same $\{p, \theta\}$ bin the fraction of accepted tracks can differ significantly between the two topologies. In order to improve the accuracy of the Monte Carlo correction and to reduce the dependence on the model used for simulation (Sec. III D), only one track topology per bin, the one with the highest acceptance, is chosen.

C. Combined particle identification

The specific ionization energy loss, dE/dx, measured in the TPCs, and the time of flight, measured with the ToF-F detectors, are used to identify charged particles of different masses in the chosen momentum intervals.

For each track, dE/dx is defined as the mean calculated from the lowest 60% of the cluster charges. This reduces the effect of the long Landau tail in the single cluster charge distribution to the extent that the dE/dx experimental

resolution can be assumed to be Gaussian within the precision which can be achieved with the available statistics.

A dedicated calibration procedure is applied to the data to correct the measured cluster charge deposits for various detector effects, e.g., charge absorption along the drift path, effective sample length, and variations of gain between the TPC sectors. After the calibration, the corrected data are fitted to a function parametrizing the Bethe-Bloch relation [18]. This function can then be used to calculate the mean dE/dx (the mean specific energy loss) for a given momentum and for a given mass hypothesis.

Kaon identification based only on the dE/dx information is impossible in the momentum bins below about 4 GeV/c, since protons and kaons have similar values of dE/dx in this kinematic range (see Fig. 3). Another approach is to identify particles through the measurement of their mass squared, m^2. This method is based on the measurement of the time of flight, which, along with the track length and momentum, allows the calculation of the particle mass.

Identification based only on the m^2 information is effective at low momenta, below about 4 GeV/c, where the separation power is higher (Fig. 3) than for dE/dx. The uncertainty on the mass measurement is in fact dominated by the time resolution, meaning that the m^2 resolution worsens quadratically with increasing momentum (Fig. 5).

Given the complementarity of the two approaches the particle identification (PID) capability can be improved, over the whole kinematic range, by using the combined dE/dx and m^2 information.

Figures 3 and 4 show distributions of measured dE/dx versus m^2 in the first angular interval, $20 < \theta < 140$ mrad, for several momentum bins. Accumulations corresponding to the different particle types are clearly observable (in particular for kaons), in contrast to the individual dE/dx and m^2 distributions.

The dE/dx-m^2 function used to fit the yields of protons (p), kaons (K^+), pions (π^+), and positrons (e^+) to the data is a superposition of four bidimensional Gaussians.

A dedicated Monte Carlo simulation was used to validate the accuracy of the simple Gaussian approximation so as to ensure that no biases related to the definition of the particle distribution function are introduced. The selected function has
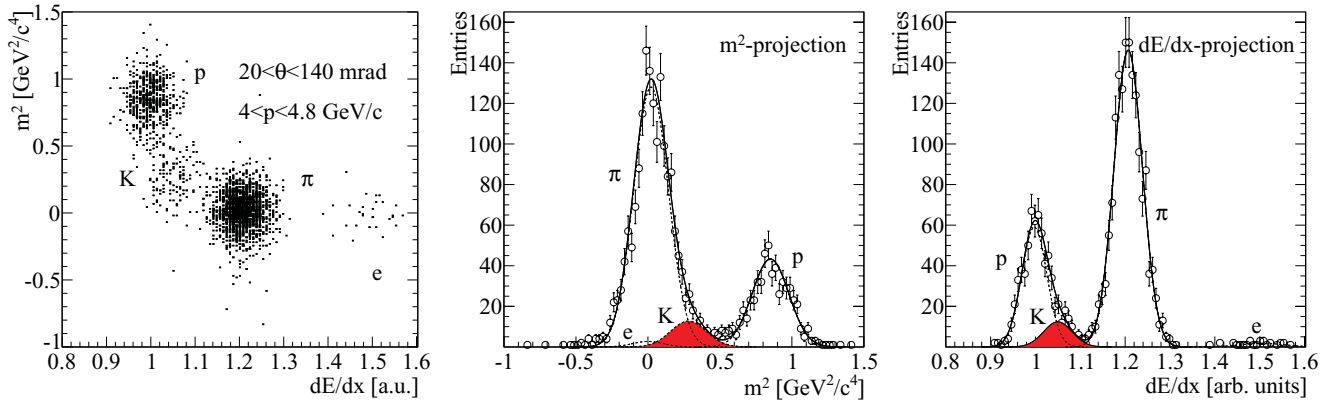
FIG. 4. (Color online) Example of a bidimensional fit to the dE/dx-m^2 distribution. The m^2 and dE/dx projections are also shown superimposed with the results of the fitted functions.

20 parameters: 4 yield, 8 width, and 8 mean parameters. In all analyzed bins the e^+ accumulations in the dE/dx-m^2 plane are fully separated from other particles (Fig. 3). Thus the number of parameters relevant for the kaon yield determination is reduced to 15. Arguments and details concerning the selected function and further reduction of the number of fitted parameters are briefly outlined below.

(i) *Width of the dE/dx distributions*: The measured width of the different dE/dx peaks is the result of the experimental (detector) resolution plus the smearing due to the variation of the dE/dx mean value with the momentum. The second contribution depends on particle type (mass) and is non-negligible in the lower momentum bins, where the relativistic rise of the energy loss is steep. In order to separate the two contributions, the variance of each Gaussian, σ_i^2 ($i \equiv p, K, \pi$), was expressed as the sum of two terms: $\sigma_i^2 = \sigma_{\exp}^2 + \sigma_{i,\mathrm{bin}}^2$. The first is the experimental resolution and is treated as a free fit parameter. The second, a constant term, was derived as the variance of the distribution of the dE/dx values calculated from the Bethe-Bloch function for all the tracks in the respective $\{p, \theta\}$ bin. Despite the fact that momentum distributions of protons, kaons, and pions differ somewhat, the momentum distribution for all particles was used to evaluate $\sigma_{i,\mathrm{bin}}^2$. This procedure was justified by Monte Carlo studies which showed that, in the considered kinematic range, a particle-type-dependent momentum distribution has no relevant impact on the outcome of the $\sigma_{p,\mathrm{bin}}^2$, $\sigma_{K,\mathrm{bin}}^2$, and $\sigma_{\pi,\mathrm{bin}}^2$ calculation.

The assumption of a resolution $\sigma_{\exp}$ independent of the particle type (mass) was validated by investigating the dependence of the dE/dx resolution on the mean dE/dx. From a fit performed to the pion distribution in bins where the accumulation is well isolated, no indication of a dependence of the peak width on the peak position was found. This result allows us to use the same experimental resolution for all hadron species.

The experimental resolution is inversely proportional to the square root of the number of dE/dx measurements for a track. The latter vary from track to track. Therefore the actual distribution of the energy loss is rather a superposition of Gaussians of different widths. The simple Gaussian approximation is still applicable since the topology of the selected tracks results in a narrow distribution of the number of points peaked above 100 in each $\{p, \theta\}$ interval. This finding was validated through a dedicated Monte Carlo simulation.

(ii) *Mean of the dE/dx distributions*: Since the mean energy loss depends only on the momentum to mass ratio, the dE/dx distributions of different particle species with the same momentum distribution are shifted. In the fit, only the pion mean energy loss was a free parameter. The kaon and proton mean parameters were instead calculated using the fitted pion mean and the shifts calculated from the Bethe-Bloch parametrization.

(iii) *Width of the m^2 distributions*: The Gaussian approximation is adopted also for the projected m^2 distributions. The Monte Carlo simulation shows that the distortion of the Gaussian shape due to the increase of the m^2 variance with the momentum has a negligible impact on the fitted yields. The m^2 width parameters of p's, K's, and π's are fitted independently.

(iv) *Mean of the m^2 distributions*: The m^2 mean parameters of p's, K's, and π's are fitted independently.

Thus the fitted parameters relevant for the kaon yield determination are three yield parameters as well as one width and one mean parameter for the dE/dx Gaussians, as well as three width and three mean parameters for the m^2 Gaussians.

Performance studies carried out on simulated data show that, in the higher momentum bins where the K/p and K/π production ratios rapidly decrease and the peaks significantly overlap, the results depend strongly on the details of the fit procedure, e.g., initial values and bounds of the fitted parameters. This in particular concerns the dE/dx and m^2 mean parameters as well as the m^2 width parameters. Along with the definition of the fit function, it is therefore mandatory to establish a procedure for the precise determination of the initial values and bounds of the fitted parameters.

For the distributions in m^2, the strategy is to estimate mean and width parameters at high momenta by extrapolating the
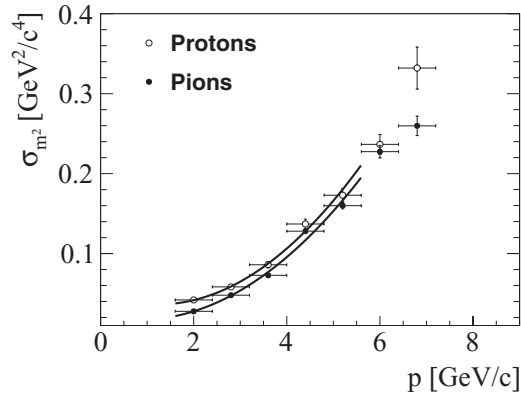
FIG. 5. The m^2 resolution vs the measured momentum for tracks with $20 < \theta < 140$ mrad. Parabolic fits to the best measured points are superimposed.

FIG. 6. Bethe-Bloch function fit to mean dE/dx values (data points). The points used in the fit are from protons and kaons of $\beta\gamma < 6$ and pions of $\beta\gamma > 20$.

fit results from low-momentum bins. First, mean parameters of protons, kaons, and pions are fitted in the bins in which particle accumulations are well separated (e.g., up to 4 GeV/c for $20 < \theta < 140$ mrad). The fitted values are independent of the momentum, which proves the correctness of the ToF-F calibration procedure. The average of the fitted mean parameters and its error are used as the initial value and bounds, respectively, in the final fit. Second, the m^2 width parameters are fitted over the whole momentum range. Figure 5 shows the results for protons and pions. As expected, the momentum dependence of the m^2 width parameter is well fitted by a second-order polynomial. The width parameter is larger for protons than for pions, since for the same momentum and path length, the time of flight is larger for heavier particles. The kaon width parameter cannot be fitted because of the small separation in m^2 of the kaon and pion Gaussians. It is therefore calculated using the fitted pion width at the momentum bin center rescaled for the correct mass value. The proton and pion resolution functions are derived via parabolic fits extended over the momentum range where peaks are well separated (e.g., up to 5.6 GeV/c for $20 < \theta < 140$ mrad; see Fig. 5). Initial values for width parameters are therefore calculated by extrapolating the resolution functions to the center of the momentum bin. Extrapolation errors are calculated as well and used to constrain the allowed fit parameter range.

Figures 3 and 4 show that in the dE/dx-m^2 plane the peak of the pion accumulation can be well determined in all analyzed bins. For protons and kaons this is possible in several bins. Thus a precise fit of the dE/dx mean parameter is possible over the whole $\beta\gamma$ range relevant for the analysis. The results are presented in Fig. 6. Points with low and intermediate $\beta\gamma$ correspond to protons and kaons while points with high $\beta\gamma$ correspond to pions. Thus, points measured with high precision are the ones with lower and higher $\beta\gamma$ while the intermediate region corresponds to protons and kaons of high momenta for which the accumulations overlap (Fig. 3).

This means that, for intermediate $\beta\gamma$ values, an accurate parametrization of the expected dE/dx can be obtained from a Bethe-Bloch curve fitted only to the high-precision measured points, which are in the low- and high-$\beta\gamma$ regions, as specified in Fig. 6.
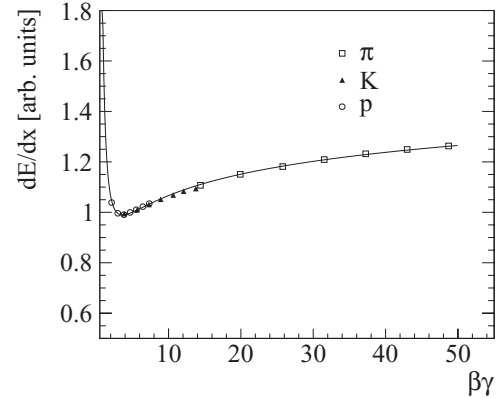
The precision of this procedure, estimated from the residuals with respect to the fit points, turned out to be about 0.5%. This value meets the requirement, derived from the Monte Carlo studies, of a precision below 1% needed to keep the systematic error below the statistical uncertainty. Estimates of the systematic errors are reported in Sec. III E. It is worth noting that the required precision on the determination of the dE/dx mean parameters cannot be achieved by using the Bethe-Bloch curve as calculated from the calibration procedure since this represents an overall parametrization of data averaged over the detector as a whole covering a wider range of track topologies.

Finally, an example of the function fitted to data using the maximum likelihood method is shown in Fig. 4.

D. Correction factors

The Monte Carlo simulation described in Refs. [8] (Sec. IV C) and [19] was used to calculate corrections for kaon decay, secondary interactions in the target and detector material, and track reconstruction efficiency. Two strategies were implemented to correct the raw spectra:

(i) The different biases were calculated separately with the Monte Carlo simulation and applied successively to the data.

(ii) A global Monte Carlo correction, taking into account all the above effects, was made.

The Monte Carlo correction factors calculated with the first strategy are shown in Fig. 7 for the first angular bin. The separation of corrections clearly shows that the decay correction dominates. This correction was estimated, for each $\{p, \theta\}$ bin, by computing the fraction of kaons produced in the primary interaction which reach the ToF-F detector array wall before decaying. As such, this procedure assumes that the track selection defined in Sec. III B, in particular the cut on the z position of the last measured point (z_{last}), is fully efficient in the isolation of a pure sample of stable kaons. Before applying this correction it is therefore necessary to correct the sample of identified kaons for the contamination from those kaons which decayed before reaching the ToF-F
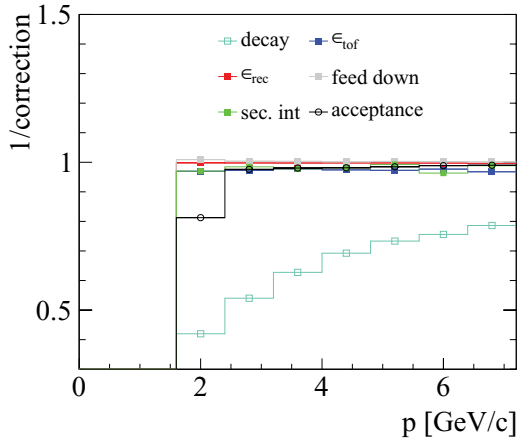
FIG. 7. (Color online) Monte Carlo correction factors as a function of momentum calculated for the angular interval $20 < \theta < 140$ mrad.

but were still associated with a ToF-F hit [see Sec. III B items (v) and (vi)]. This contamination was found to be of about 2%–3%.

The feed-down correction concerns kaon tracks fitted to the primary vertex but not produced in the primary interaction. Feed down is only observed from kaons produced by secondary interactions in the target and the effect is below 2% over the whole kinematic range.

The ToF-F detector efficiency was accounted for and calculated from the data by requiring that a track traversing the ToF-F detector array wall generates a hit in the ToF-F detector.

Except for the first momentum bin, the small correction for geometrical acceptance (on top of the factor due to the selection of the ϕ wedge) reflects the fact that only full acceptance regions were selected, as described in Sec. III B. Tracks are also required to hit the ToF-F detector array. For these long tracks the reconstruction efficiency is close to unity.

The contribution related to kaon losses due to secondary interactions in the detector material is about 2%.

Within the second strategy, global correction factors were calculated by means of different detector response unfolding methods [20]. All the applied methods returned results whose discrepancies are significantly below the associated statistical errors.

Correction factors obtained through the unfolding technique were compared to those calculated as the product of the individual factors derived from method (i). Results turned out to be compatible within the statistical fluctuations and no systematic biases were observed. This implies that all the relevant contributions to the corrections were identified and quantified correctly and that the different contributions are weakly correlated. Moreover, since the unfolding procedure accounts for event migration between adjacent bins, the compatibility of the two approaches proves that bin-by-bin correlation of the correction factors is negligible as well.

E. Systematic errors

The main contribution to the overall systematic error on the yield correction arises from the decay correction.

Three main contributions to the systematic uncertainty of the decay correction are discussed below.

(i) *The contribution due to kaons decaying in flight*: Most of the unstable kaons in the selected final sample are decays which take place in the region of space delimited by z_{last} and the ToF-F detector array surface. An alternative way to derive the decay correction is then to calculate the survival probability only until $z = z_{last}$. In this procedure one must correct for the small contamination of kaons decaying between z_{last} and the ToF-F detector array which are not associated with a ToF-F hit. The two methods give results which differ by less than 1%. The systematic error assigned to the bias related to kaon decays was therefore conservatively calculated as 50% of the corresponding contamination (see Sec. III D).

(ii) *The contribution due to the model dependence of momentum distributions*: The value of the decay correction depends on the momentum distribution within each $\{p, \theta\}$ bin and therefore on the specific Monte Carlo model used for the event generation. Significant discrepancies may be observed especially at low momenta where the decay probability (the correction) is larger and the momentum distribution is steeper. This effect was quantified by using various Monte Carlo models and comparing the resulting correction factors with those calculated directly from the data. More precisely, the latter factor was derived for the three lowest momentum bins, where unique identification of kaons is possible on a track-by-track basis: the raw yield was corrected by reweighting each track with its decay probability, calculated for the measured momentum and track length. The resulting deviation of the correction factor was negligible except in the first momentum bin where a maximum difference of about 2% was found.

(iii) *The contribution due to the uncertainty in the reconstructed track length*: Since only well-measured tracks which traverse the entire spectrometer are retained, a precision of a few millimeters is achieved on both track length calculation and extrapolation to the ToF-F detector array surface. This translates into a negligible (order of 0.1%) error on the decay correction factor.

Other sources of systematic errors include uncertainties on the ToF-F and reconstruction efficiency and on the contribution from secondary interactions. Systematic uncertainties on the ToF-F detector array efficiency come from the accuracy of the calibration procedure. The estimated value is 2%. The systematic error on the reconstruction efficiency was estimated by varying the track selection cuts. The induced bias is small compared to the statistical fluctuations; this is expected given the high reconstruction efficiency. Finally, a systematic error corresponding to 30% of the correction was assigned to the contribution of secondary interactions [8].

Systematic uncertainties related to the procedure used for the PID (Sec. III C) were quantified by studying the dependence of the fitted kaon yields on the input fit parameters, namely, the central values of the dE/dx and m^2 distributions and the widths in m^2. The systematic error was obtained by
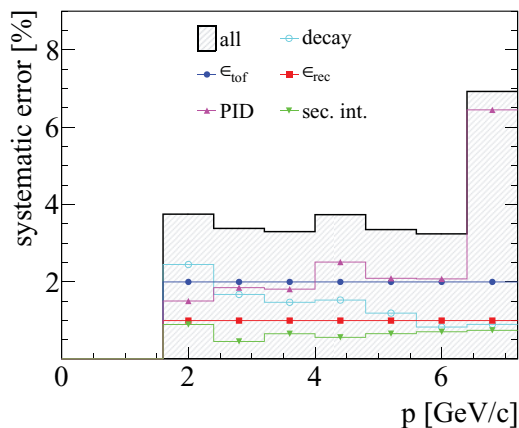
FIG. 8. (Color online) Breakdown of systematic errors as a function of momentum for the angular interval $20 < \theta < 140$ mrad.

varying both the input parameters and limits and considering the subsequent variation of the returned particle yield.

In particular, the relative distances of the proton, kaon, and pion dE/dx peaks were varied by an amount corresponding to the largest of the residuals between the fitted Bethe-Bloch curve and the measured points (see Sec. III C). The allowed range for the m^2 peak position and resolution were enlarged by a factor of 3 with respect to the original value which had been derived from the errors in the parametrization as described in Sec. III C. Results are shown in Fig. 8.

As underlined in the introduction of Sec. III, the sensitivity to the kaon signal decreases with the momentum; therefore, the fitted kaon yield depends significantly on the definition of the input parameters. This explains the steep increase of the systematic error in the last momentum bin.

The relative contributions of all considered systematic errors are shown in Fig. 8 for the first angular interval.

IV. RESULTS

The K^+ spectra presented in this paper refer to positively charged kaons produced in strong and electromagnetic processes in $p + C$ interactions at 31 GeV/c. Differential inclusive K^+ cross sections were derived following the procedure described in Refs. [8,21]. The results are presented in Fig. 9 and Table I as a function of momentum in the two considered intervals of polar angle. Momentum and polar angle are calculated in the laboratory system.

The ratio of K^+ to π^+ production cross sections is shown in Fig. 10. The π^+ spectra, measured with the same dataset used for the present kaon analysis, are taken from Ref. [8], and central values and errors are recalculated to match the binning used in the current analysis. Numerical values are reported in Table I.

V. COMPARISON WITH MODEL PREDICTIONS

In this section we compare the K^+ spectra in $p + C$ interactions at 31 GeV/c with the predictions of hadronic event generators. Three models, VENUS4.12 [22,23], FLUKA2008 [24],
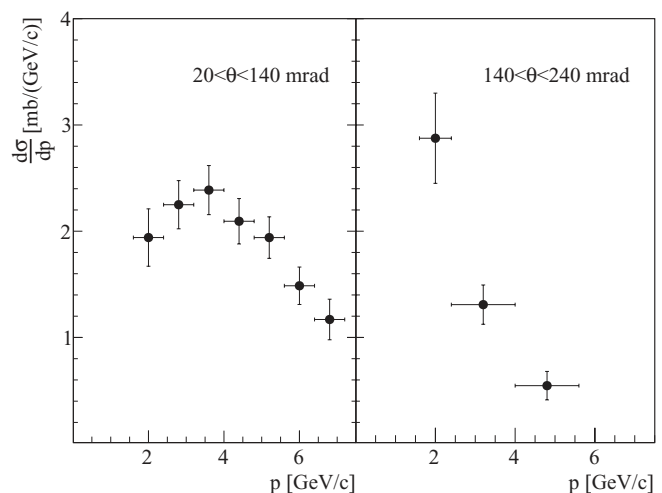

FIG. 9. Differential cross sections for K^+ production in $p + C$ interactions at 31 GeV/c. The spectra are presented as a function of laboratory momentum, p, in two intervals of polar angle, θ. Error bars indicate statistical and systematic uncertainties added in quadrature. The overall uncertainty (2.5%) due to the normalization procedure is not included.

and URQMD1.3.1 [25,26], were selected for this purpose. They are part of the CORSIKA [27] framework and are commonly used for the simulation of hadronic interactions at energies below 80 GeV in extensive air showers [28]. VENUS is also the standard model for acceptance simulations of the NA49 and NA61 Collaborations.

These models were already compared to the pion spectra measured by the NA61/SHINE Collaboration [8]. Motivated by this comparison, Uzhinsky [26] proposed a correction for a technical shortcoming of the URQMD model. However, this correction relates to a phase-space region (i.e., $0 < \theta < 20$ mrad and $p < 1.5$ GeV/c) which is not covered by the
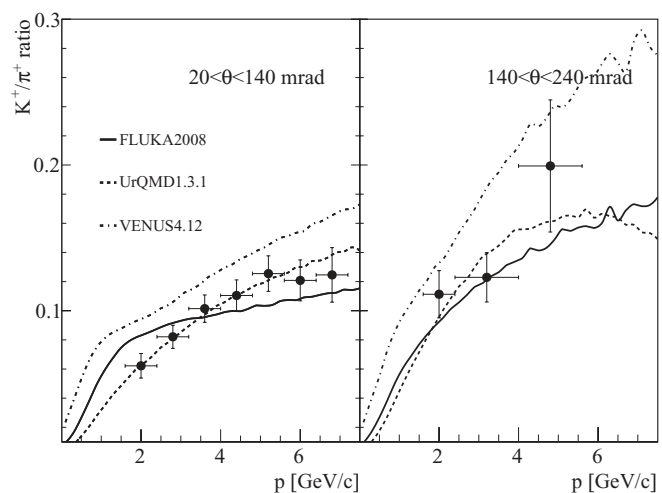

FIG. 10. Ratio of K^+ to π^+ production cross sections in $p + C$ interactions at 31 GeV/c. The ratios are presented as a function of laboratory momentum, p, in two intervals of polar angle θ. Errors are calculated by taking into account only statistical uncertainties. Predictions of hadron production models are superimposed.
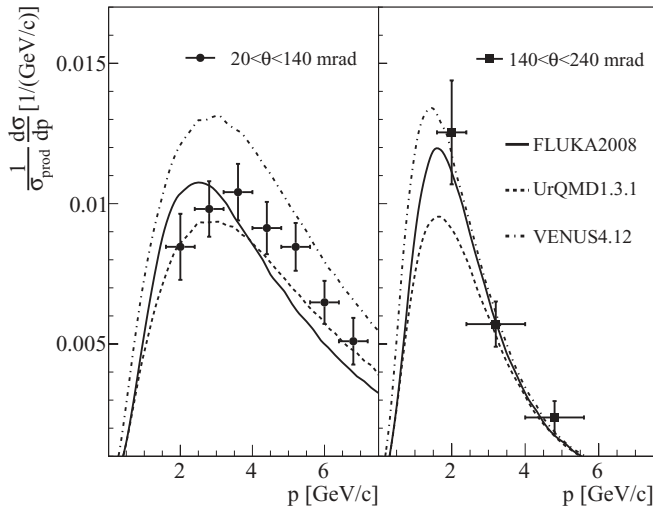
FIG. 11. Comparison of measured K^+ spectra with model predictions. Distributions are normalized to the mean K^+ multiplicity in all production $p + C$ interactions. The vertical error bars on the data points show the total (stat. and syst.) uncertainty. The horizontal error bars indicate the bin size in momentum.

kinematic range of this analysis, and therefore we compare our measurements with the original implementation.

The results of the comparison between data and models are presented in Fig. 11. In order to avoid uncertainties related to the different treatments of the quasielastic interaction and to the absence of predictions for inclusive cross sections, the spectra are normalized to the mean K^+ multiplicity in all production interactions. For the data, the normalization relies on the $p +$ C inclusive production cross section σ_{prod}, which was found to be $229.3 \pm 1.9 \pm 9.0$ mb. The production cross section is calculated from the inelastic cross section by subtracting the quasielastic contribution. Therefore, production processes are defined as those in which only new hadrons are present in the final state. Details of the cross section analysis procedure can be found in Refs. [8,21].

The qualitative behavior of the data is well reproduced by all models. The quantitative differences can be related to the two main production processes of kaons: pairwise production of a K^+ together with another K meson and production of a K^+ together with a Λ baryon. The latter process dominates kaon production at large momenta and small angles due to the leading particle effect. K^+ production at large angles and low momenta stem from pair production of K mesons. Both FLUKA and VENUS provide a reasonable description of the pair-produced kaons. On the other hand, none of the models is in full agreement with the small-angle data. While the VENUS model overestimates the production of K^+ at small angles, FLUKA and URQMD predict a slightly lower kaon production rate.

Figure 10 also shows the comparison between models and data for the ratio of K^+ to π^+ production cross sections: URQMD is in good agreement with the data, FLUKA provides a reasonable description, while VENUS overestimates the production cross section ratio for both small and large angle intervals.

VI. SUMMARY

This work presents measurements of differential production cross sections of positively charged kaons in $p + $ C interactions at 31 GeV$/c$. These data are essential for precise predictions of the high-energy tail and intrinsic electron neutrino component of the initial neutrino flux for the T2K long-baseline neutrino oscillation experiment in Japan. Furthermore, they provide important input to improve hadron production models needed for the interpretation of air showers initiated by ultra-high-energy cosmic particles. The measurements were performed with the large-acceptance NA61/SHINE spectrometer at the CERN SPS. A set of data collected with a 4% λ_{I} isotropic graphite target during the pilot NA61/SHINE run in 2007 was used for the analysis. Positively charged kaon spectra as a function of laboratory momentum in two intervals of the polar angle were obtained. The final spectra were compared with predictions of hadron production models. The data presented in this paper are already provided to T2K for the calculation of the neutrino flux. Meanwhile, a much larger data set with both the thin (4% λ_{I}) and the T2K replica carbon targets was recorded in 2009 and 2010 and is presently being analyzed.

[1] N. Antoniou *et al.* (NA49-future Collaboration), CERN-SPSC-2006-034, 2006.

[2] N. Antoniou *et al.* (NA61/SHINE Collaboration), CERN-SPSC-2007-004, 2007.

[3] N. Antoniou *et al.* (NA61/SHINE Collaboration), CERN-SPSC-2007-019, 2007.

[4] N. Abgrall *et al.* (NA61/SHINE Collaboration), CERN-SPSC-2008-018, 2008.

[5] K. Abe *et al.* (T2K Collaboration), Nucl. Instrum. Methods, Phys. Res., Sect. A **659**, 106 (2011).

[6] J. Abraham *et al.* (Pierre Auger Collaboration), Nucl. Instrum. Methods, Phys. Res., Sect. A **523**, 50 (2004).

[7] T. Antoni *et al.* (KASCADE Collaboration), Nucl. Instrum. Methods A, Phys. Res., Sect. **513**, 490 (2003).

[8] N. Abgrall *et al.* (NA61/SHINE Collaboration), Phys. Rev. C **84**, 034604 (2011).

[9] K. Abe *et al.* (T2K Collaboration), Phys. Rev. Lett. **107**, 041801 (2011).

[10] T. Abbott *et al.*, Phys. Rev. D **45**, 3906 (1992).

[11] Y. D. Aleshin *et al.*, ITEP-80-1977, 1977.

[12] J. V. Allaby *et al.*, CERN Report **70-12**, 1970.

[13] D. Dekkers *et al.*, Phys. Rev. **137**, 962 (1965).

[14] T. Eichten *et al.*, Nucl. Phys. B **44**, 333 (1972).

[15] G. J. Marmer *et al.*, Phys. Rev. **179**, 1294 (1969).

[16] I. A. Vorontsov *et al.*, ITEP-88-011, 1988.

[17] S. Murphy, Ph.D. thesis, University of Geneva (in preparation).

[18] R. M. Sternheimer and R. F. Peierls, Phys. Rev. B **3**, 3681 (1971).

[19] N. Abgrall, Ph.D. thesis, University of Geneva, 2011.

[20] T. Adye, Proceedings of the PHYSTAT 2011 Workshop, CERN, Geneva, arXiv:1105.1160.

[21] C. Strabel, Ph.D. thesis, ETH Zurich, 2011.

[22] K. Werner, Nucl. Phys. A **525**, 501 (1991).

[23] K. Werner, Phys. Rep. **232**, 87 (1993).

[24] G. Battistoni *et al.*, AIP Conf. Proc. **896**, 31 (2007); for consistency we show FLUKA2008.3 in the comparison. This is the same version of FLUKA used in the T2K analysis [9] and the analysis of the pion data [8]. However, FLUKA2008.3 is no longer distributed since the release of FLUKA2011.2. FLUKA2011.2 contains some modifications to the high-energy hadron-nuclear models which could impact the model prediction in the energy range of the measurements reported here.

[25] S. A. Bass *et al.*, Prog. Part. Nucl. Phys. **41**, 255 (1998).

[26] V. Uzhinsky, arXiv:1107.0374 [hep-ph] (2011).

[27] D. Heck *et al.*, Report Forschungszentrum Karlsruhe FZKA-6019, 1998.

[28] H.-J. Drescher, M. Bleicher, S. Soff, and H. Stoecker, Astropart. Phys. **21**, 87 (2004).